Observing the prevalence of thin current sheets downstream of Earth's bow shock

I. Gingell,[1] S. J. Schwartz,[2] H. Kucharek,[3] C. Farrugia,[3] and K. J. Trattner[2]

[1)] *School of Physics and Astronomy, University of Southampton, Southampton, SO17 1BJ, UK*

[2)] *Laboratory for Atmospheric and Space Physics, University of Colorado, Boulder, Colorado 80303, USA*

[3)] *Space Science Center, University of New Hampshire, Durham, New Hampshire 03824, USA*

(*Electronic mail: i.l.gingell@soton.ac.uk)

(Dated: 22 September 2021)

Actively reconnecting, thin current sheets have been observed both within the transition region of Earth's bow shock and far downstream into the magnetosheath. Irrespective of whether these structures arise due to shock processes or turbulent dissipation, they are expected to contribute to particle heating and acceleration within their respective regions. In order to assess the prevalence of thin current sheets in the magnetosheath, we examine shock crossings and extended magnetosheath intervals recorded by the Magnetospheric Multiscale mission (MMS). For each magnetosheath interval we quantify the prevalence of current sheets in that region of space using: a one-dimensional measure of structures per unit length of observed plasma, a packing factor corresponding to the fraction of time the spacecraft are within current structures, and a three-dimensional measure requiring an estimate of the number of current sheets within an associated volume. We estimate that volume by considering the three-dimensional cone over which Alfvén and magnetoacoustic waves can propagate during each interval. Using 25 extended magnetosheath intervals observed by MMS, we perform our analysis for different locations in the magnetosheath and for different solar wind conditions. We find that the number density of current sheets is higher towards the magnetosheath flanks, that it reduces as a power law with distance from the bow shock, and that it is not strongly influenced by the properties of the upstream bow shock.

I. INTRODUCTION

The magnetosheath region of Earth's magnetosphere, comprising shocked solar wind plasma bounded by the bow shock and the magnetopause, is observed to be a turbulent medium[1–5]. In turbulent plasmas, nonlinear interactions form coherent, intermittent structures, such as thin current sheets, which are linked to energy dissipation[6]. Multiple kinetic processes are expected to contribute to energy dissipation in collisionless plasma turbulence, including magnetic reconnection at intermittent current structures[7–11]. To identify and characterise signatures of reconnection at thin current sheets, such as fast outflows, we require *in situ* observation using high-resolution plasma instrumentation. In the turbulent magnetosheath, reconnection at thin current sheets has therefore been observed with both Cluster[12–14] and the Magnetospheric Multiscale mission (MMS)[15–18]. Recently, thin current sheets in the magnetosheath have also been seen to undergo "electron-only" reconnection, for which only an electron outflow is observed[17] with no corresponding ion outflow. Turbulent regions for which electron-only reconnection has been observed have also been shown to exhibit differences in the character of the turbulence[19].

Similarly, observations by MMS have shown that magnetic reconnection also occurs at thin current sheets within the transition region of Earth's bow shock[20–22]. Kinetic simulations of these processes reveal that reconnection at shocks can occur by at least two mechanisms: Weibel instabilities causing filamentation in the shock foot[23], and steepening of upstream waves driven by stream instabilities[24,25]. Magnetic islands generated by the latter mechanism are observed to propagate downstream of the shock ramp. Observational surveys of reconnection at the bow shock[22] suggest that reconnection at thin current sheets is localised to shock, such that the prevalence of reconnecting current sheets reduces downstream. However, this survey was designed to focus on shock reconnection only—it did not select intervals for which the spacecraft spent significant time in the magnetosheath.

The observation of thin current sheets within both the turbulent magnetosheath and the transition layer of the bow shock therefore raises the questions of whether and how these phenomena are related. For example, reconnection at thin current sheets in the magnetosheath may be the end state of processes which generate thin current sheets at the bow shock. Alternatively, current sheet generation and associated energy repartition may operate differently in each region. In order to explore any differences, we must perform a survey of thin current sheets across the full extent of the bow shock transition region and the magnetosheath, effectively extending downstream the survey of the shock performed by Gingell *et al*[22]. By quantifying the number (and number density) of current sheets observed in different regions of the magnetosheath, we can constrain mechanisms for sheet generation, and infer the integrated effect of energy repartition processes across the full population of current sheets. This supports previous work in quantifying energy repartition at current sheets by Schwartz *et al*[26], who found for one case study close to the subsolar point that current sheets repartition 5-10% of the incident solar wind flow energy.

In this paper, we extend surveys of thin current sheets across the full magnetosheath, identifying these structures for 25 extended magnetosheath crossings by the Magnetospheric Multiscale spacecraft. We describe several methods for estimating packing factor, one-dimensional and three-dimensional number density of these thin current sheets. Finally, we examine the dependence of these packing factors and number densities on bow shock and magnetosheath parameters.

II. OBSERVATIONS

In order to survey kinetic-scale current structures in the magnetosheath we required extended periods of (ideally) uninterrupted, high-resolution *in situ* field and plasma data captured by the Magnetospheric Multiscale mission (MMS)[27]. Electromagnetic field data are provided by MMS's flux gate magnetometer (FGM)[28] and electric field double probe (EDP)[29,30], both within the FIELDS suite of instruments[31]. The FGM magnetic fields are sampled at 128 Hz, and the EDP electric fields are sampled at 8 kHz. Particle data are provided by the Fast Plasma Investigation (FPI)[32]. The full three-dimensional ion phase space is sampled by FPI's Dual Ion Spectrometer (DIS) every 0.15s, and the electron phase space is sampled by the Dual Electron Spectrometer (DES) every 0.03s. Upstream solar wind parameters, including solar wind speeds, interplanetary magnetic field (IMF) and plasma beta are provided by OMNI, and are time shifted to the bow shock.

The analysis described in this paper has been performed for 25 individual magnetosheath intervals, encompassing all those recorded in high-resolution burst mode for at least 15 minutes each during the period December 2017 to March 2020. Continuous magnetosheath crossings that have been captured in burst mode for an hour or more have been split into smaller intervals of approximately 20-30 minutes. Interval times and mean plasma parameters for all analysed crossings are given in Table I. The locations of the spacecraft during each interval are shown in Figure 1. These intervals span much of the magnetosheath close to the ecliptic plane ($Z_{GSE} = 0$), including both

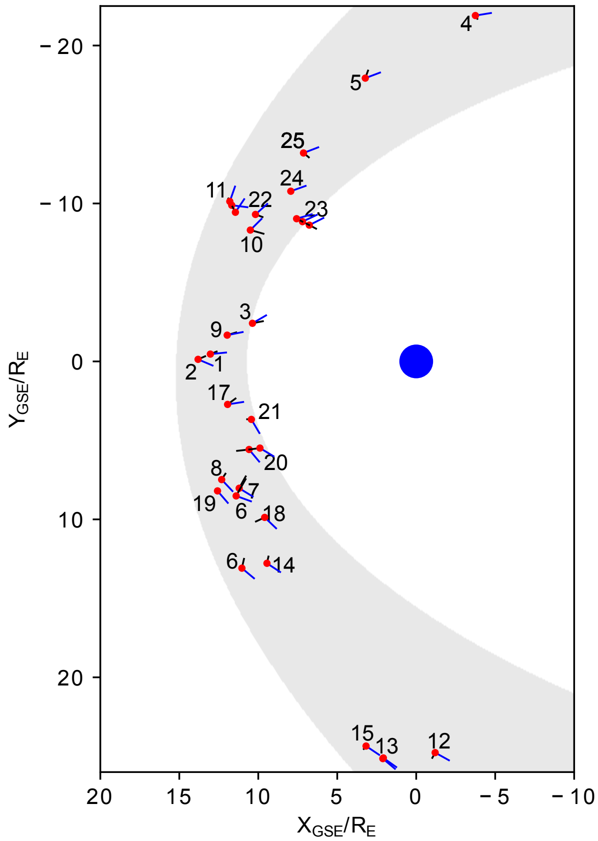

FIG. 1. Spacecraft trajectories (black) for MMS1 for each of the numbered magnetosheath intervals in Table I, projected onto the $Z_{GSE} = 0$ plane. Blue lines show the direction (not the magnitude) of the bulk velocity for each interval. Red dots show the end of each interval. The grey area is bounded on the sunward side by the model bow shock[33] and the earthward side by the model magnetopause[34], both for average solar wind conditions.

flanks and the subsolar point. An overview of interval 2, a quasi-parallel magnetosheath crossing, is shown in Figure 2. Frequent magnetic field reversals corresponding to current sheets are observed in panel (a), chiefly in the B_Z component. Field and plasma parameters are observed to be broadly constant during this interval, consistent with a low variability in the incoming solar wind. An overview of interval 3, a quasi-perpendicular magnetosheath crossing, is also shown in Figure 3. Although far fewer thin current sheets are observed in Figure 3 than for the quasi-parallel magnetosheath in Figure 2, we note that this is not necessarily typical.

TABLE I. Times and associated mean plasma parameters for extended magnetosheath intervals included in this analysis. The shock orientation θ_{Bn} and Mach number $M_{A,up}$ are calculated using upstream plasma parameters from OMNI. The ion and electron plasma beta $\beta_{i,e}$ are given for the magnetosheath from direct MMS observation. Given poor OMNI coverage for interval 2, the shock orientation for that interval is calculated using the given period and the following hour, during which the upstream conditions are stable.

	Date	Interval (UTC)	Shock Crossing (UTC)	θ_{Bn} (deg)	$M_{A,up}$	β_i	β_e
1	2017-12-21	06:41:54 - 07:03:53	07:49:46	32 ± 6	16.5	25.6	4.0
2	2017-12-21	07:21:53 - 07:48:03	07:49:46	$32 \pm 7^*$	28.4	10.3	1.5
3	2017-12-26	19:49:13 - 20:17:23	21:50:30	82 ± 7	11.8	17.6	1.5
4	2018-04-19	05:08:04 - 05:41:52	06:08:10	76 ± 8	16.4	15.2	3.4
5	2018-04-23	07:50:14 - 08:33:42	05:37:00	52 ± 7	9.0	4.6	0.9
6	2018-11-21	16:10:14 - 16:55:32	17:16:00	56 ± 5	6.4	3.9	0.7
7	2018-11-29	22:42:34 - 23:31:02	23:36:00	43 ± 18	13.2	7.0	2.3
8	2018-12-05	14:53:24 - 15:20:12	15:22:00	29 ± 10	8.9	13.5	1.9
9	2019-01-11	03:22:24 - 03:52:22	04:04:40	30 ± 6	7.9	13.3	2.3
10	2019-02-12	14:33:04 - 15:17:52	15:19:50	19 ± 8	7.1	12.1	2.2
11a	2019-04-05	11:11:04 - 11:23:22	10:55:30	48 ± 1	6.3	12.7	1.2
11b	2019-04-05	11:30:54 - 11:38:22	10:55:30	41 ± 2	6.8	2.4	0.7
11c	2019-04-05	11:43:24 - 12:05:22	10:55:30	34 ± 4	6.9	1.8	0.5
12	2019-11-15	00:17:34 - 01:06:02	00:16:00	86 ± 4	21.9	5.3	1.5
13a	2019-11-22	00:09:24 - 00:12:52	00:09:20	85 ± 3	7.6	4.7	1.6
13b	2019-11-22	00:17:24 - 00:19:32	00:21:30	83 ± 5	7.2	6.0	1.2
14	2019-11-23	11:46:24 - 12:13:12	13:23:30	47 ± 12	4.1	3.5	1.0
15	2019-11-25	13:17:34 - 13:46:32	13:49:35	67 ± 13	9.9	5.0	0.8
16	2019-12-07	09:33:44 - 10:39:22	11:03:00	27 ± 7	7.8	3.2	0.6
17	2019-12-28	08:22:54 - 08:53:22	09:22:12	28 ± 15	17.0	20.4	3.3
18	2020-01-14	05:21:54 - 05:52:42	05:17:57	36 ± 10	13.9	9.6	1.7
19	2020-01-24	16:55:14 - 17:01:52	17:03:05	34 ± 5	14.0	11.0	2.8
20a	2020-02-04	07:26:14 - 08:00:42	06:26:00	45 ± 8	12.7	8.7	1.1
20b	2020-02-04	08:00:44 - 08:30:12	06:26:00	45 ± 5	9.8	6.7	1.4
21	2020-02-14	20:56:54 - 21:08:22	20:05:34	26 ± 3	17.5	7.0	1.0
22	2020-02-26	00:23:54 - 00:49:12	01:20:20	30 ± 5	8.3	8.5	2.0
23a	2020-02-29	09:58:04 - 10:20:02	11:01:55	43 ± 7	8.8	2.0	0.3
23b	2020-02-29	10:20:04 - 10:42:02	11:01:55	38 ± 8	10.8	4.4	0.7
23c	2020-02-29	10:42:04 - 11:01:32	11:01:55	37 ± 8	10.3	17.3	2.6
24	2020-03-07	12:31:34 - 12:40:22	12:43:00	60 ± 7	10.6	10.5	1.3
25	2020-03-18	02:05:24 - 02:30:12	02:31:20	28 ± 9	9.1	6.9	1.2

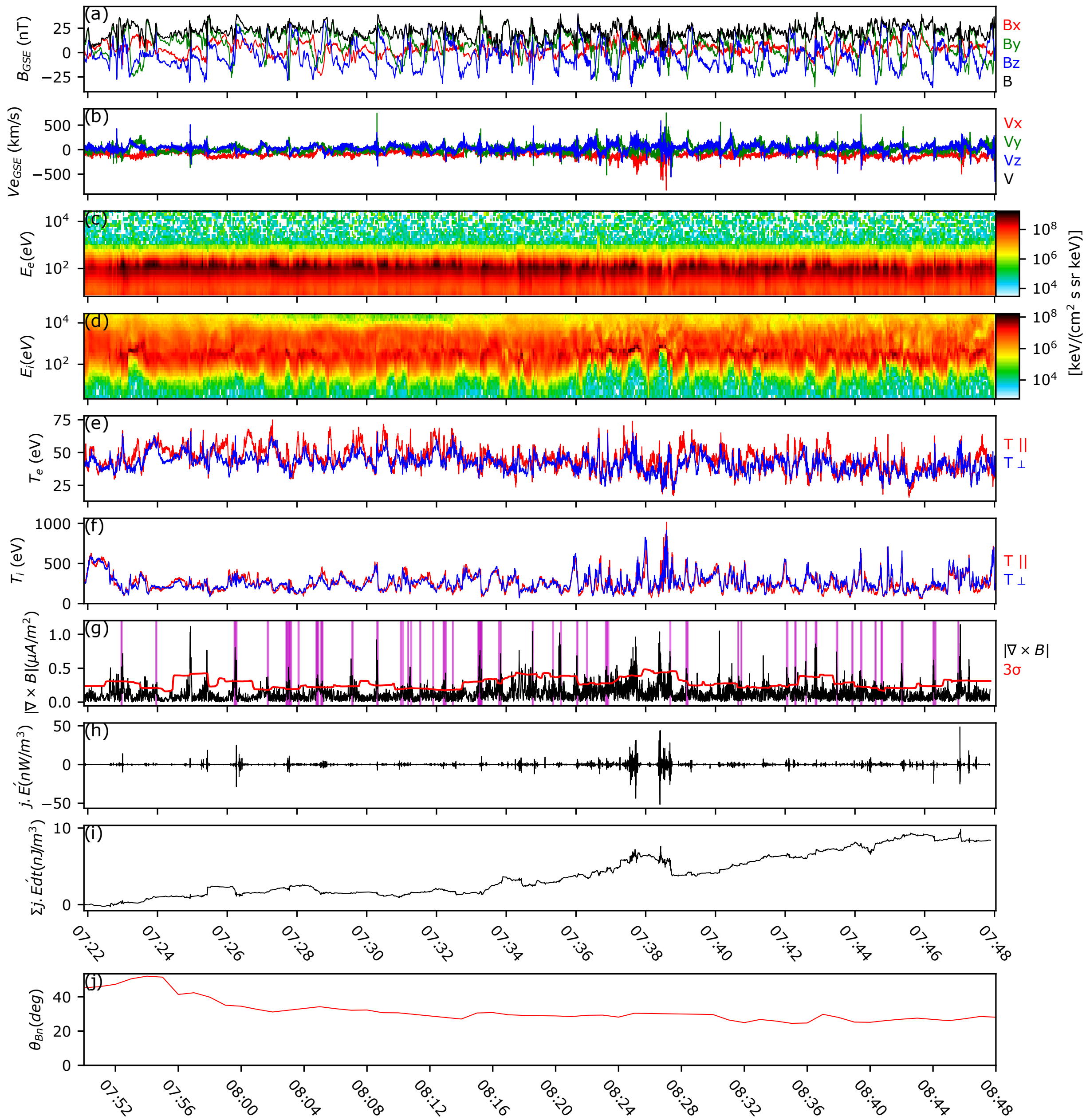

FIG. 2. Summary of the extended quasi-parallel magnetosheath crossing observed by MMS1 during interval 2, 2017-12-21 07:21:53 - 07:48:03 UTC: (a) FGM magnetic fields, (b) electron bulk velocity, (c), omnidirectional electron energy spectrogram, (d) omnidirection ion energy spectrogram, (e) electron temperature, (f) ion temperature, (g) magnitude of the current density from the curlometer method (black), showing 3σ criteria (red) and regions that exceed the threshold (magenta), (h) $\mathbf{j} \cdot \mathbf{E}'$, (i) integrated $\mathbf{j} \cdot \mathbf{E}'$, (j) θ_{Bn} from the upstream conditions observed by OMNI.

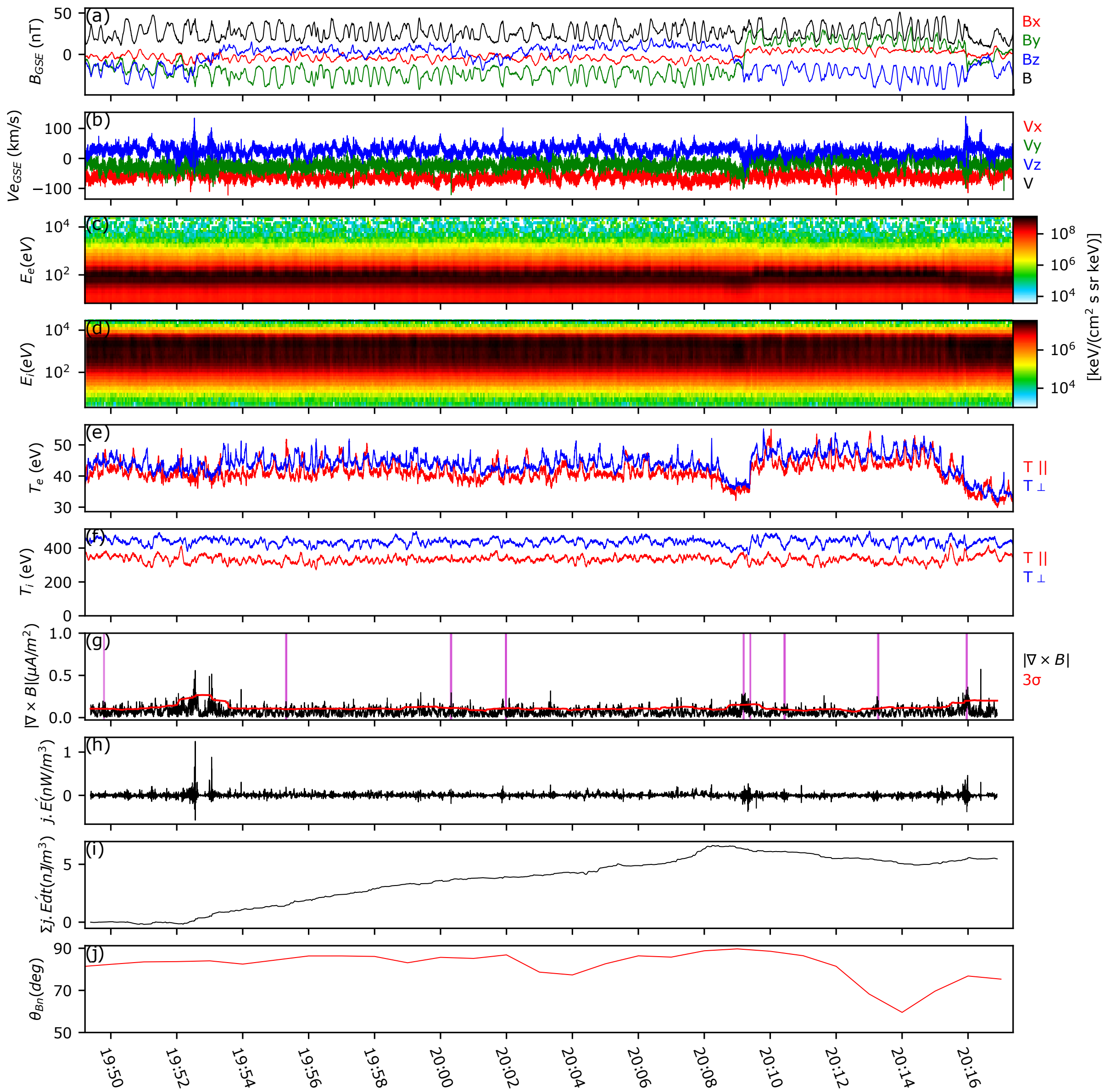

FIG. 3. Summary of the extended quasi-perpendicular magnetosheath crossing observed by MMS1 during interval 3, 2017-12-26 09:49:13 - 20:17:23 UTC: (a) FGM magnetic fields, (b) electron bulk velocity, (c), omnidirectional electron energy spectrogram, (d) omnidirection ion energy spectrogram, (e) electron temperature, (f) ion temperature, (g) magnitude of the current density from the curlometer method (black), showing 3σ criteria (red) and regions that exceed the threshold (magenta), (h) $\mathbf{j}\cdot\mathbf{E}'$, (i) integrated $\mathbf{j}\cdot\mathbf{E}'$, (j) θ_{Bn} from the upstream conditions observed by OMNI.

A. Identifying Current Sheets

For each magnetosheath interval, a survey of current structures is performed in a manner similar to that described by Gingell *et al*[22]. First, the current density is calculated using the FGM magnetic fields, requiring multi-point measurements of the field with all four MMS spacecraft[35]. The magnitude of the current density is shown for Interval 2 in Figure 2(g). Possible intervals of interest likely to contain a current structure are identified first as any region for which the magnitude of the current density is greater than a given threshold $|J(t)| > N\sigma_J(t)$. The standard deviation of the current density at a given time $\sigma_J(t)$ is calculated for data in the range $t \pm 30$s. The following analysis has been performed for thresholds at $N = [1,2,3,4,5]$. We note that the 3σ threshold $N = 3$ has been used in previous studies[22,26]. Possible intervals are then combined if they fall within 0.2s of each other. The time-dependent current density threshold with $N = 3$ is shown for Interval 2 in Figure 2(g) as a red line.

To assess whether each identified interval of high current density contains a current sheet, we first perform a minimum variance analysis using the magnetic field (MVAB)[36] and transform into the local LMN coordinate system, where L is the maximum variance direction and N is the minimum variance direction. A current structure is then recorded as a current sheet if the following additional criteria are met. First, the LMN coordinate system must be well defined: the eigenvalue ratios λ_L/λ_M and λ_M/λ_N must both exceed 3. Second, the maximum variance component of the magnetic field B_L observed by MMS1 must change sign across the current carrying region. Time intervals that fulfil all these conditions for current density threshold $N = 3$ are shown for interval 2 in Figure 2(g) as magenta shaded regions. In contrast to Gingell *et al*[22], we do not require the presence of an electron jet or outflow, i.e. we are not seeking signatures of active magnetic reconnection. While this approach may also lead to the selection of other current structures such as flux ropes, we expect these structures to be a small minority for threshold $N = 3$ and above, as is the case for the magnetosheath crossing reported by Schwartz *et al*[26].

III. ESTIMATING SHEET DENSITY

The simplest method of estimating the prevalence of current sheets in the magnetosheath is to count the number of current sheets observed within a given interval:

$$n_{\mathrm{cs,1D}} = \frac{N_{cs}}{\langle v_{\mathrm{bulk}} \rangle \Delta t}, \quad (1)$$

where N_{cs} is the number of current sheets identified by the survey described in Section II A, $\langle v_{\text{bulk}} \rangle$ is the mean bulk electron speed, and Δt is the duration of the magnetosheath interval. This is a one-dimensional measure of current sheet 'density', i.e. the number of current sheets observed per unit length in the plasma rest frame.

We also estimate the 'packing factor' of current sheets p_{cs} as follows:

$$p_{cs} = \frac{\sum_i \delta t_i}{\Delta t}, \tag{2}$$

where δt_i is the time interval corresponding to the current carrying region of a current sheet i. The quantity p_{cs} is therefore the fraction of the time series (or trajectory) occupied by current sheets. We note that the relationship between this one-dimensional packing factor and the three-dimensional packing factor is strongly dependent on the geometry of the current sheets. The one- and three-dimensional packing factors will converge for all cases only if current sheets are strongly planar structures which extend the full system size along their tangential dimensions.

A. Three-Dimensional Measures

Here we describe an alternative quantification of the number density of current sheets which is intended to account for the three-dimensional packing and distribution of the current sheets. For this measure, we seek an estimate of the number of current sheets within a volume rather than along a trajectory. In this case, the number density of current sheets n_{cs} is given by:

$$n_{\text{cs,3D}} = \frac{N'_{\text{cs}}}{V_{\text{cone}}} \tag{3}$$

where N'_{cs} is an estimate of the number of current sheets within a given volume V_{cone}. Obtaining an estimate of n_{cs} therefore requires two separate calculations: i) the volume of a region of interest corresponding to a given time interval, and ii) the number of current sheets that influence the plasma during that time interval.

For each magnetosheath interval given in Table I, this calculation of the number density of current sheets is repeated for a sliding window of maximum duration $\Delta t = D_{sh}/v_{\text{bulk}}$, where D_{sh} is the estimated distance to the bow shock from the spacecraft along the vector $-\mathbf{v}_{\text{bulk}}$. In this way, we assume that current structures and their indirect effects originate at or downstream of the bow shock. For each magnetosheath interval, the position of the bow shock (and hence the distance along $-\mathbf{v}_{\text{bulk}}$) is estimated by using a bow shock model[33] scaled to the shock crossing observed closest in time to that interval. The times of these nearest shock crossings are given for each magnetosheath interval in Table I. We note that since the nearest shock crossings are recorded minutes to hours before or after the intervals of interest, it is possible that there are significant errors in D_{sh} due to the dynamic response of the bow shock to the upstream conditions, including the effects of non-stationarity and instabilities in the foreshock that can occur even during otherwise steady solar wind conditions. The results reported for each magnetosheath interval in Section IV are the mean of the results from each sliding window sub-interval taken for that magnetosheath crossing.

1. Volume of Influence

The volume associated with a given time interval is taken to be an "Alfvén cone", analogous to a light cone. This corresponds to the volume within which an Alfvénic or fast magnetoacoustic disturbance could intersect the spacecraft trajectory since the start of the time interval. Given the bulk velocity of the plasma v_{bulk}, the interval duration Δt, and taking the speed of propagation parallel and perpendicular to the field lines as the Alfvén speed v_A and fast magnetoacoustic speed v_{fast} respectively, the volume of the Alfvén cone is therefore:

$$V_{\text{cone}} = \frac{\pi}{3}\Delta t^3 v_{\text{bulk}} v_{\text{A}} v_{\text{fast}} \sin(\theta_{Bv}), \tag{4}$$

where θ_{Bv} is the angle between the magnetic field and the bulk plasma velocity. The magnetic field, bulk velocity and wave speeds are taken as the mean values across the chosen interval. This volume is illustrated in Figure 4. We note that the length of the cone, given by $v_{bulk}\Delta t$ and shown as a blue solid line in Figure 4, corresponds to the spacecraft trajectory in the plasma rest frame; it is not the length of the spacecraft trajectories in the GSE coordinate system shown as black trails in Figure 1.

2. Number of Current Sheets

The number of sheets N'_{cs} associated with the volume V_{cone} is intended to account for the current sheets directly encountered by MMS, and any within the volume V_{cone} that are not directly observed, but that nevertheless contribute to changes in the observed plasma properties across the magnetosheath. This total is estimated by dividing the total change in certain plasma measures by the mean change of those measures recorded at directly observed current sheets, i.e. those

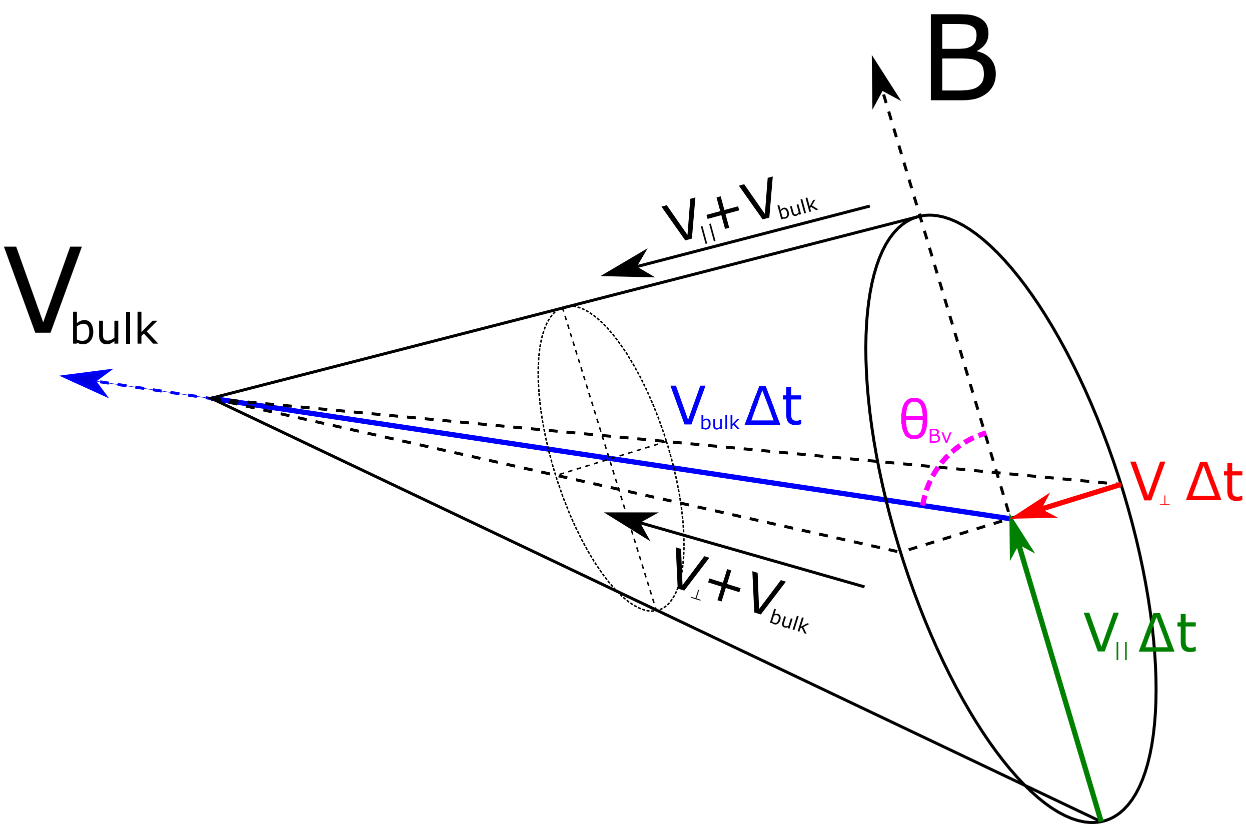

FIG. 4. Illustration of the Alfvén influence cone volume, given the bulk velocity $\mathbf{v}_{\text{bulk}}$, magnetic field vector $\mathbf{B}$, angle between those two vectors θ_{Bv}, time interval Δt, and parallel and perpendicular propagation velocities $v_{\|}$ and $v_{\perp}$. In this case, the parallel propagation speed $v_{\|}$ is given by the Alfvén speed v_A, and the perpendicular propagation speed $v_{\perp}$ is given by the fast magnetoacoustic speed v_{fast}. The solid blue line corresponds to the spacecraft trajectory in the plasma rest frame, covering the distance $v_{\text{bulk}}\Delta t$.

recorded by the survey described in Section II A. Estimates of the number of currents sheets N'_{cs} are derived here from two plasma measures, each of which are correlated with energization of plasma within current sheets: the magnetic inflow energy, and $\mathbf{j}\cdot\mathbf{E}'$.

a. Magnetic Inflow Energy We can estimate the number of current sheets by considering the magnetic inflow energy associated with each structure, $E_{\text{inflow}} = m_i v^2_{AL,\text{inflow}}$. The asymmetric Alfvén inflow speed is given by:

$$v^2_{AL,\text{inflow}} = \frac{B_{L,1}B_{L,2}\left(B_{L,1}+B_{L,2}\right)}{\mu_0(\rho_1 B_{L,2}+\rho_2 B_{L,1})}. \tag{5}$$

Subscripts 1 and 2 denote the regions either side of the current carrying region, B_L is the maximum variance component of the magnetic field, and ρ is the ion mass density[17].

An empirical survey of the magnetopause by Phan *et al*[37] showed that the change in the electron temperature due to reconnection at current sheets is related to the magnetic inflow energy by $\delta T_e \approx 0.017 E_{\text{inflow}}$. Case studies by Phan *et al*[17], Gingell *et al*[20] and Wang *et al*[21] have shown that this relationship holds for reconnection at thin current sheets in the magnetosheath and the transition region of the bow shock. We can therefore estimate the number of current sheets within the volume of influence by dividing the total change in the electron temperature across the full interval ΔT_e by the mean of the temperature change expected for individual current sheets in that interval $\langle \delta T_e \rangle$:

$$N'_{\text{cs}} = \frac{\Delta T_e}{0.017 \langle E_{\text{inflow}} \rangle}. \tag{6}$$

The overall change in the electron temperature ΔT_e is calculated by first performing a linear fit to the temperature time series across the (sliding window) magnetosheath interval, then recording the temperature change of the linear fit over the interval duration. We use this approach to ensure that our ΔT_e measure is not unduly affected by small-scale, local inhomogeneities.

By characterising thin current sheets by their magnetic inflow energy in this way, we have assumed that the magnetic inflow energies of current sheets identified by the survey are representative of those that have or will transfer that energy to the particles via magnetic reconnection in the magnetosheath. Given that other instabilities and wave-particle interactions can lead to heating or energy transfer in the magnetosheath, Equation 6 represents an overestimate of the three-dimensional number density of current sheets associated with each time interval. Schwartz *et al*[26] demonstrate for one magnetosheath crossing that isolated current structures convert field to particle energy at a rate comparable to the change in enthalpy flux across the magnetosheath. However, different regions of the magnetosheath or different solar wind conditions may lead to a lesser (or greater) fraction of energy conversion by current sheets. For example, if 50% the increase in the electron temperature is attributable to current sheets, the number density of current sheets should be approximately 50% of that determined using Equation 6. Hence, the three-dimensional number density of current sheets presented in this study can only be considered an upper bound.

b. j.E' We can also estimate the number of current sheets by considering the quantity $\mathbf{j} \cdot \mathbf{E}'$, where $\mathbf{E}' = \mathbf{E} + \mathbf{v}_e \times \mathbf{B}$. Positive $\mathbf{j} \cdot \mathbf{E}'$ corresponds to the exchange of energy from the electromagnetic fields to the particles in the particle rest frame.

For a time series $f(t)$ corresponding to $\mathbf{j} \cdot \mathbf{E}'$, the total integrated $\mathbf{j} \cdot \mathbf{E}'$ across a (sliding window) magnetosheath interval from t_0 to t_1 is given by $\int_{t_0}^{t_1} f(t)\, dt$. We next assume that all changes in this cumulative $\mathbf{j} \cdot \mathbf{E}'$ are attributable to processes at thin current sheets. We can therefore estimate the number of current sheets responsible for this cumulative change in $\mathbf{j} \cdot \mathbf{E}'$ by dividing it by the mean of the change within the current sheets observed during that same interval:

$$N'_{\rm cs} = \frac{\int_{t_0}^{t_1} f(t)\,dt}{\left\langle \int_{t_{0,i}}^{t_{1,i}} f(t)\,dt \right\rangle}, \qquad (7)$$

where $t_{0,i}$ to $t_{1,i}$ is the time interval corresponding to the current carrying region of an individual current sheet i. Given that other instabilities and wave-particle interactions can lead to energy transfer in the magnetosheath, Equation 7 represents an overestimate of the three-dimensional number of current sheets associated with each time interval. As with Equation 6, the three-dimensional number density of current sheets estimated using this method can only be considered an upper bound.

We note two further caveats in using the quantity $\mathbf{j}\cdot\mathbf{E}'$ for this method. First, instrument calibrations for MMS require that the parallel electric field averages to zero. Hence, long-term integration of the electric field via $\mathbf{j}\cdot\mathbf{E}'$ may be unreliable. Second, $\mathbf{j}\cdot\mathbf{E}'$ can only quantify local particle energisation. This stands in contrast to the magnetic inflow energy method discussed above, since observed increases in electron temperature can include thermalisation of plasma in regions that are not directly intersected by the spacecraft trajectory. Hence, while this $\mathbf{j}\cdot\mathbf{E}'$ method is unlikely to produce as reliable a result as the magnetic inflow energy method, it can nevertheless serve as a useful point of comparison: the $\mathbf{j}\cdot\mathbf{E}'$ method will only include the effects of current sheets along or very close to the spacecraft trajectory.

IV. RESULTS

The one-dimensional number density of current sheets $n_{\rm cs,1D}$ and packing factor $p_{\rm cs}$, described by Equations 1 and 2 respectively, are shown for the chosen magnetosheath intervals in Figure 5. We observe one-dimensional number densities of approximately $n_{\rm cs,1D} \approx 10^{-4}{\rm km}^{-1}$ to $10^{-3}{\rm km}^{-1}$, and packing factors $p_{\rm cs}$ of approximately 1% to 5%. The top panels of Figure 5 show the relationship between the distance from the bow shock and the one-dimensional number density (left, red) or packing factor (right, blue). The distance to the shock D_{sh} is taken along the bulk velocity vector, and the shock location is calculated from the Peredo *et al*[33] model scaled to the nearest shock crossing observed by MMS. We observe negative correlations between the distance from the shock and both the one-dimensional number density and the packing factor. In each case, dashed lines demonstrate best fit power-laws with index $\alpha = -0.33$ and $\alpha = -0.17$ for the number density and packing factor respectively. However, with a correlation coefficient of only $|R| \approx 0.5$, these relationships are considered weak.

Figure 5 also shows the relationship between the number density of current sheets (and packing factor) and two bow shock parameters: the Alfvén Mach number M_A (middle row) and orientation of the bow shock θ_{Bn} (bottom row). The shock angle given here, $\theta_{Bn,v}$, corresponds to the angle between the upstream magnetic field and the shock normal at the intersection of the bow shock and the vector $-\mathbf{v}_{\rm bulk}$, again calculated from the Peredo *et al*[33] model scaled to the nearest shock crossing observed by MMS. For all combinations, we observe no clear relationship between the one-dimensional number density of current sheets or packing factor and the shock parameters M_A and θ_{Bn}. Given the lack of dependence of number density or packing factor on θ_{Bn}, it appears that the magnetosheath downstream of the quasi-parallel shock ($\theta_{Bn} < 45°$) does not host more current sheets than the magnetosheath downstream of the quasi-perpendicular shock ($\theta_{Bn} > 45°$).

Before discussing trends in the three-dimensional measures of the number density of current sheets $n_{\rm cs,3D}$ outlined in Section III A, we first examine its dependence on the current sheet identification method described in Section II A and illustrated for interval 2 in Figure 2(g). Figure 6 shows the observed number densities $n_{\rm cs}$ for several different values of N, corresponding to the current density magnitude threshold in event identification, i.e. $|J(t)| > N\sigma_J(t)$. We find that the data lie approximately along the trend $n_{\rm cs,3\sigma} = n_{\rm cs,N\sigma}$ (shown as a dashed line), with a relatively weak systematic offset for which the densities $n_{\rm cs}$ calculated using higher thresholds (e.g. $N = 5$) are at most twice as high as those using lower thresholds (e.g. $N = 1$). This systematic offset can arise due to the weaker currents with larger scale lengths being combined during the sheet identification process. Given that we observe trends in $n_{\rm cs,N\sigma}$ across several orders of magnitude, this systematic difference is relatively weak. Hence, the trends we identify in $n_{\rm cs}$ are not strongly dependent on current density thresholds. This in turn implies that most current sheet intervals identified with lower current density thresholds (e.g. $N = 1$) contain current sheet intervals identified with higher current density thresholds (e.g. $N = 5$), and that each structure's contribution to the magnetic inflow energy and integrated $\mathbf{j}\cdot\mathbf{E}'$ is largely contained within the region of highest current density. For all subsequent results, we report number densities based on the identification criteria $|J(t)| > 3\sigma_J(t)$, i.e. $N = 3$.

For the magnetosheath intervals given in Table I, the three-dimensional number densities of current sheets span several orders of magnitude, from $n_{\rm cs,3D} \approx 10^{-2}{\rm km}^{-3}$ to $10^{-12}{\rm km}^{-3}$. We note that the highest recorded three-dimensional number densities $n_{\rm cs} \approx 10^{-2}{\rm km}^{-3}$ are unreal-

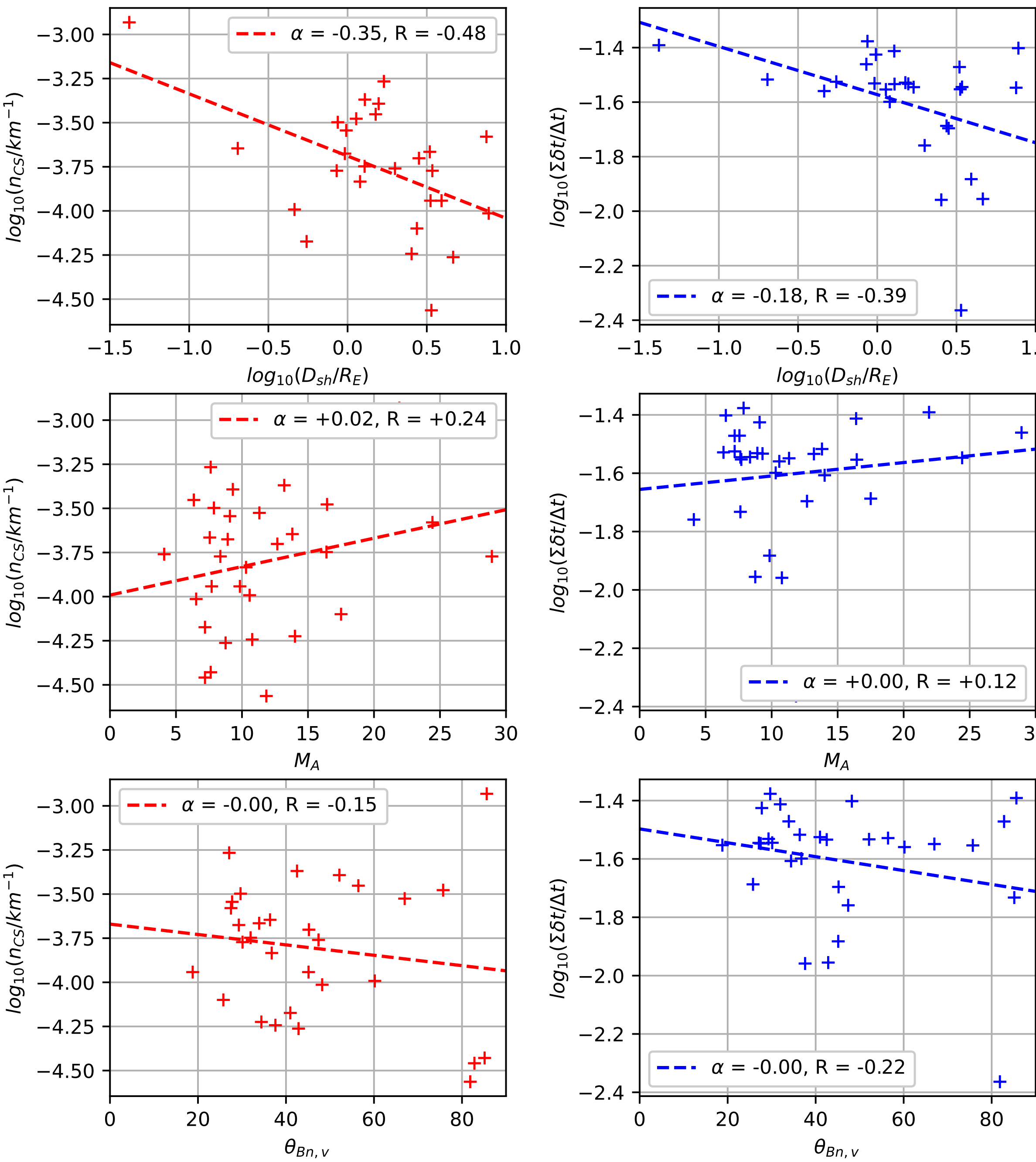

FIG. 5. The relationship between the one-dimensional number density of current sheets $n_{\rm cs}$ (left column, red) or the packing factor $p_{cs} = \Sigma\delta t/\Delta t$ (right column, blue) and the distance from the shock (top row), Alfvén Mach number (middle row) and shock orientation θ_{Bn} (bottom row). Lines correspond to linear fits with gradient α and correlation coefficient R.

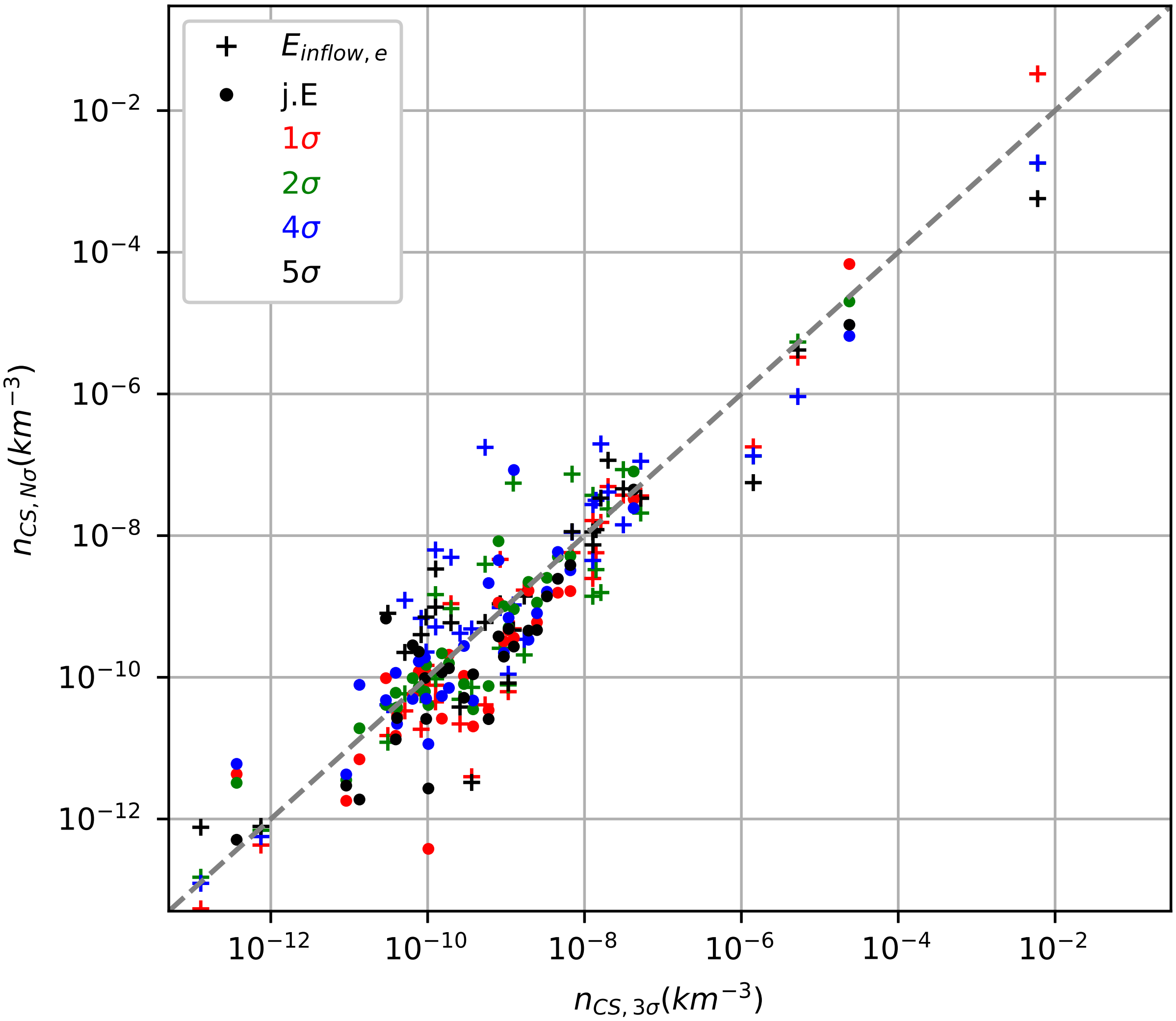

FIG. 6. The relationship between the three-dimensional number density of current sheets n_{cs} calculated using different current density magnitude thresholds N, with associated condition $|J(t)| > N\sigma_J(t)$. The standard measure $n_{\text{cs},3\sigma}$ is plotted against $n_{\text{cs,N}\sigma}$ for $N = [1,2,4,5]$, for methods based on magnetic inflow energy ('+' markers) and $\mathbf{j}\cdot\mathbf{E}'$ ('o' markers). A dashed line represents the relationship $n_{\text{cs},3\sigma} = n_{\text{cs,N}\sigma}$.

istically high. For ion inertial length $d_i \approx 50$km, this corresponds to approximately 10^3 current structures per cubic ion inertial length. However, for the majority of the magnetosheath intervals we record number densities between $n_{\text{cs}} \approx 10^{-7}\text{km}^{-3}$ and 10^{-12}km^{-3}, corresponding to more reasonable estimates of $10^{-2}d_i^{-3}$ to $10^{-7}d_i^{-3}$. We also note that the three-dimensional number density of current sheets is typically larger than the cube of the one-dimensional number density (with $n_{\text{cs,3D}} \approx 10^{-9}\text{km}^{-3}$ and $n_{\text{cs,1D}} \approx 10^{-3.5}\text{km}^{-1}$). This may indicate that the tangential extent of the current sheets, i.e. their length along the L and M directions for each sheet, is less than the typical separation between current sheets along the spacecraft trajectory in the plasma rest frame. In contrast, if current sheets had large tangential extent (or infinite tangential extent, for an effectively 2D system), the three-dimensional number density would be observed to be much less than the cube of the one-dimensional number density. Again we stress that the three-dimensional number densities given in this study are considered upper bounds.

Figure 7 shows the relationship between the three-dimensional number density of current sheets $n_{\rm cs}$ and the location of each magnetosheath interval. The location in the magnetosheath is characterised by two distances: the distance to the shock along the bulk velocity vector D_{sh}, and the magnitude the Y-coordinate in GSE (right panel). We observe a clear power law trend in the current sheet density as a function of distance from the shock, $n_{\rm cs} \propto D_{sh}^{\alpha}$, where $\alpha \approx -2.6$ to -4. This power-law drop in the sheet density downstream of the shock supports the findings of the survey by Gingell *et al*[22] that reconnecting structures are most common in the region closest to the shock ramp, reducing through the shock transition region and into the magnetosheath. The trend is supported by both magnetic inflow energy and $\mathbf{j} \cdot \mathbf{E}'$ methods, with correlation coefficients $|R| \approx 0.9$ in both cases. We note that in capping the maximum length of the Alfvén cone at the distance to the bow shock (see Section III A) the maximum sliding window duration Δt is proportional to the distance to the shock, and so $V_{\rm cone} \propto \Delta t^3 \propto D_{sh}^3$. Hence, if we were to observe the same rate of current sheets per unit time no matter the distance from the shock (i.e. $N'_{\rm cs} \propto \Delta t$), we would observe a shallower power law index of $\alpha \approx -2$.

We also observe an exponential increase in current sheet number density with $|Y_{GSE}|$, outwards from the subsolar point to the magnetosheath flanks and increasing by an order of magnitude over approximately $5R_E$. However, the correlation between $|Y_{GSE}|$ and the current sheet number density is weaker, with $R \approx 0.6$.

We explore the relationship between the number density of current sheets and upstream shock parameters in Figure 8. Weak positive correlations are observed between $n_{\rm cs}$ and shock orientation θ_{Bn}. However, we note that there are relatively few data corresponding to magnetosheath intervals behind quasi-perpendicular shocks. Omitting points for which $\theta_{Bn} > 80^{\circ}$, we find no clear relationship between bow shock orientation and current density in the magnetosheath. As with the one-dimensional measures in Figure 5, this lack of dependence of current sheet number density on θ_{Bn} suggests that the magnetosheath downstream of the quasi-parallel shock does not host more current sheets than the magnetosheath downstream of the quasi-perpendicular shock.

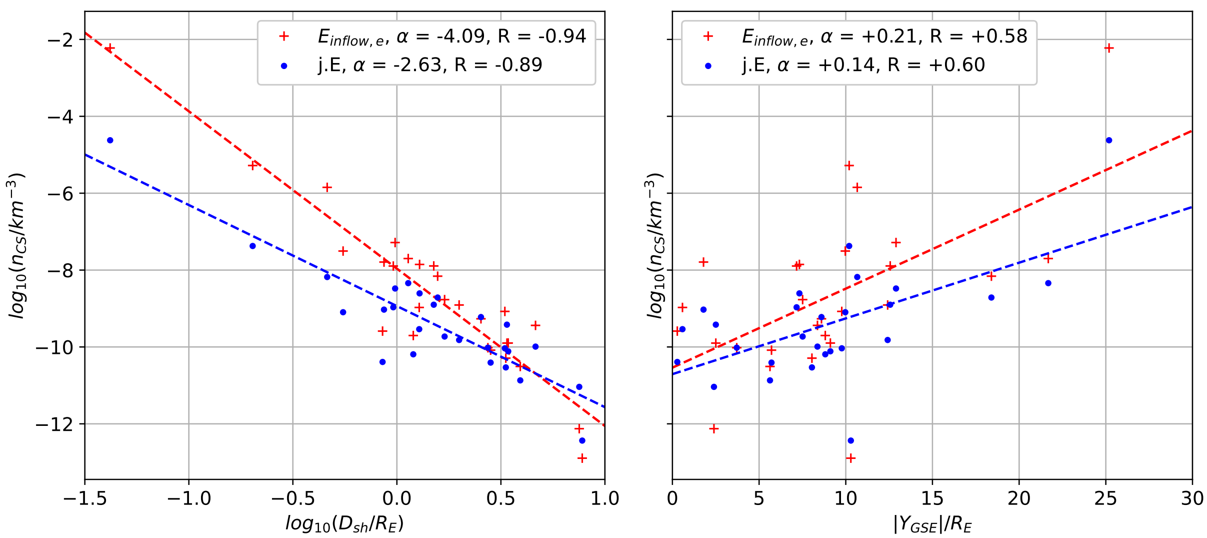

FIG. 7. The relationship between the three-dimensional number density of current sheets n_{cs} and location in the magnetosheath. Distance along the bulk velocity vector to the shock (left) and absolute distance from $|Y_{GSE}|$ (right) are shown for both magnetic inflow energy (red) and $\mathbf{j}\cdot\mathbf{E}'$ (blue) counting methods. Lines correspond to linear fits with gradient α and correlation coefficient R.

Similarly, we observe very weak or no correlation between n_{cs} and upstream Alfvén Mach number M_A. Together these demonstrate that the three-dimensional number density of current sheets is not strongly dependent on bow shock parameters.

The relationships between the number density of the current sheets and mean magnetosheath plasma parameters are shown in Figure 9, including ion and electron plasma beta β_i and β_e. As with the shock parameter relationships shown in Figure 8, we find no clear trend between the magnetosheath parameters and the number density of current sheets.

Finally, we note that the $\mathbf{j}\cdot\mathbf{E}'$ method consistently under-estimates the number density relative to the magnetic inflow energy by approximately an order of magnitude. This is clearly visible in the trends for Figures 7, 8 and 9, for which the blue fit lines ($\mathbf{j}\cdot\mathbf{E}'$) are generally lower than the red fit lines (magnetic inflow energy). This is consistent with the assumptions of each method. As noted in section III A, the $\mathbf{j}\cdot\mathbf{E}'$ method can only capture localised energisation along the spacecraft trajectory, whereas the magnetic inflow energy method can capture non-local thermalisation of the plasma. The magnetic inflow energy method will therefore account for current sheets within the broader volume of influence, and in turn record a significantly higher number density n_{cs}. However, it is also important to recognise that particle energisation captured by integration of

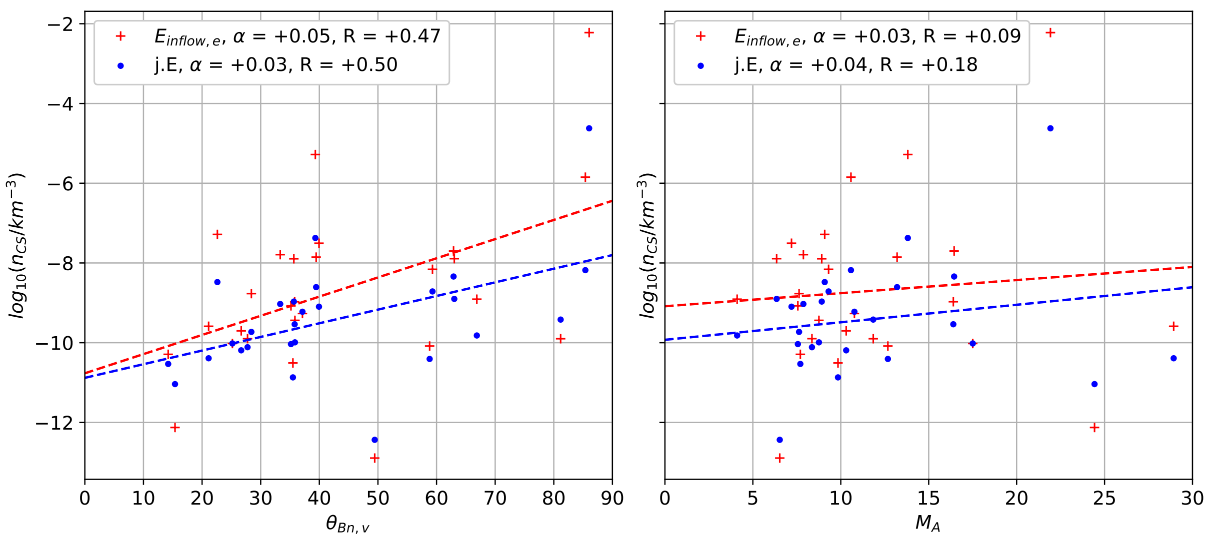

FIG. 8. The relationship between the three-dimensional number density of current sheets $n_{\rm cs}$ and shock parameters upstream of the intervals of interest. Angle between the shock normal and upstream magnetic field θ_{Bn} (left) and Alfvén Mach number M_A (right) are shown for both magnetic inflow energy (red) and $\mathbf{j}\cdot\mathbf{E}'$ (blue) counting methods. Lines correspond to linear fits with gradient α and correlation coefficient R.

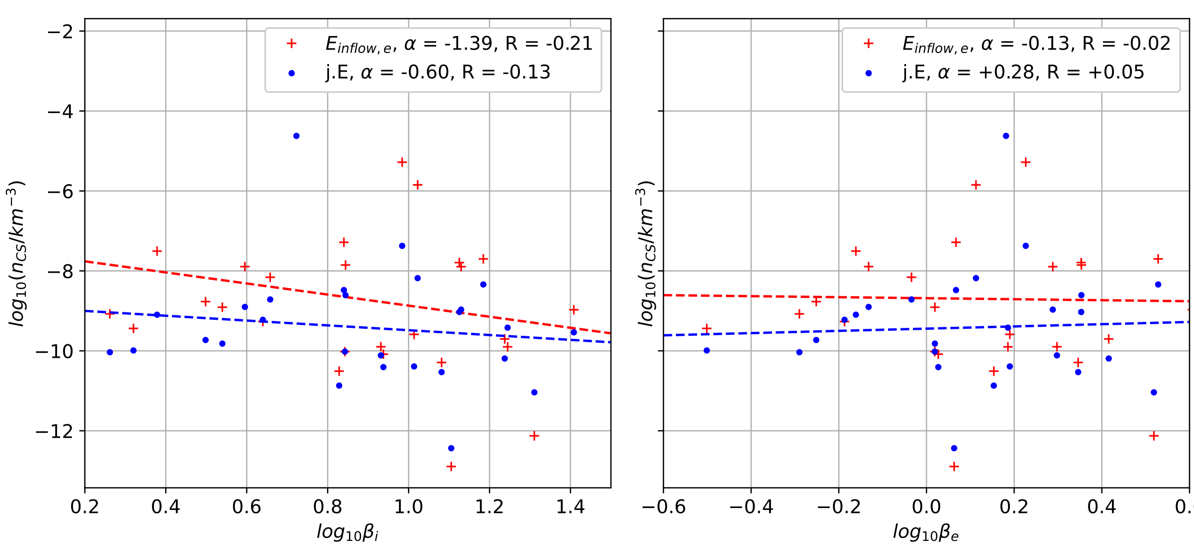

FIG. 9. The relationship between the three-dimensional number density of current sheets $n_{\rm cs}$ and magnetosheath conditions. Ion plasma beta β_i (left) and electron plasma beta β_e (right) are shown for both magnetic inflow energy (red) and $\mathbf{j}\cdot\mathbf{E}'$ (blue) counting methods. Lines correspond to linear fits with gradient α and correlation coefficient R.

$\mathbf{j}\cdot\mathbf{E}'$ may include structures that are *not* captured by electron temperature differences used for the magnetic inflow energy method, and vice versa. Indeed, as discussed in Section III A the three-dimensional number density of current sheets calculated with both methods can be considered approximate upper bounds.

V. CONCLUSIONS

In this study we have performed a broad survey of current structures associated with > 20 minute crossings of the magnetosheath by Magnetospheric Multiscale. For each of the 25 intervals we have identified current sheets by searching for times during which the magnitude of the current density exceeds a given threshold, then selecting those for which the maximum variance component of the magnetic field reverses. We have quantified the number density of current sheets first using a simple one-dimensional measure: the number of current sheets observed within a given time interval. We also measure the 'packing factor', corresponding to the fraction of the time series associated with current sheet crossings. Finally, we perform a three-dimensional measure of the number density of current sheets by calculating a volume of influence for each interval based on the Alfvén and magnetoacoustic wave travel time, and then estimating the total number of current sheets that influence the plasma in that volume.

We record one-dimensional number densities of current sheets of approximately $n_{cs,1D} \approx 10^{-4}\mathrm{km}^{-1}$ to $10^{-3}\mathrm{km}^{-1}$, and packing factors of approximately 1% to 5%. The three-dimensional number density varies by several orders of magnitude across the magnetosheath, typically between $n_{\mathrm{cs,3D}} \approx 10^{-7}\mathrm{km}^{-3}$ and $10^{-12}\mathrm{km}^{-3}$. An order-of-magnitude difference between the densities quantified using $\mathbf{j}\cdot\mathbf{E}'$ and magnetic inflow energy metrics suggests that the Alfvén cone method cannot produce a reliable magnitude for the current sheet number density. However, we do observe similar trends in the densities recorded for both $\mathbf{j}\cdot\mathbf{E}'$ and magnetic inflow energy metrics, suggesting that this Alfvén cone method remains useful for evaluating relative densities and magnetospheric trends.

We do not observe any significant dependence of any measures of the prevalence of current sheets on either the upstream shock parameters θ_{Bn} and M_A, or on the magnetosheath plasma beta. This suggests that processes at the shock (or in the sheath) that generate current sheets are not strongly dependent on shock (or sheath) conditions within the parameter ranges typically observed at Earth.

More specifically, the magnetosheath behind the quasi-parallel bow shock ($\theta_{Bn} < 45^\circ$) does not appear to host more current sheets than the magnetosheath behind the quasi-perpendicular bow shock ($\theta_{Bn} > 45^\circ$), despite the quasi-parallel shock typically exhibiting more disordered and non-stationary structure. This is consistent with statistical studies of reconnecting current sheets in the shock transition region[22], and supports the conclusion that generation of current sheets by shock processes is universal. However, we also note that unexpectedly low prevalence of current sheets on the quasi-parallel side of the magnetosheath may instead be a consequence of the current sheet identification criteria. If the quasi-parallel magnetosheath is more disordered or turbulent, current sheets may be embedded in local inhomgeneities or combined with other current structures, in turn causing them to fail to identification requirements such as a reversal of B_L across the current carrying region. Indeed, Yordanova *et al*[38] demonstrated a significant increase in the apparent number of current sheets in a quasi-parallel magnetosheath compared to the quasi-perpendicular region during the same magnetosheath crossing. The differing conclusions between these studies may reflect the differences in methods for current sheet identification, differences in quantification of current sheet prevalence, and differences between the plasma parameters and solar wind conditions of each individual magnetosheath interval.

Most importantly, we observe strong correlation between the three-dimensional number density of current sheets $n_{\mathrm{cs,3D}}$ and the location of magnetosheath crossing intervals with respect to the global magnetosphere. A weaker correlation is also observed for the one-dimensional number density $n_{\mathrm{cs,1D}}$ and packing factor. Specifically, we identify a power law $n_{\mathrm{cs,3D}} \propto D_{sh}^{\alpha}$, where $\alpha \approx -3$ to -4 and D_{sh} is the distance to the bow shock. That is, the number density of current sheets is generally much higher in regions close to the bow shock. The negative correlation between distance to the bow shock and the three-dimensional measure of current sheet number density is significantly stronger than between the distance to the bow shock and the one-dimensional measure: $R_{1D} \approx -0.5$, and $R_{3D} \approx 0.9$. Furthermore, we identify a weaker positive correlation between the three-dimensional current sheet number density and the magnitude of the Y_{GSE} coordinate of the interval location: current sheets appear to be more common in the magnetosheath flanks than at the subsolar point. This may be a consequence of a different character of the magnetic fluctuations and turbulence in the flanks compared to the subsolar region[4]. For example, large, ion-scale current sheets as part of a well-developed turbulence in the flanks may be more easy to detect using our algorithm than electron-only reconnection sites nearer the subsolar point. Further study will be required to investigate the cause of this apparent trend.

Together these trends reveal that the generation (and decay) of current sheets varies considerably in different regions of the magnetosheath. The influence of current sheets on the local plasma environment is known to be important across multiple scales: current sheets can serve to generate disordered or turbulent fluctuations at large scales[39], and are also expected to play a role in the dissipation of energy at the smallest scales[7–11]. Furthermore, current sheets may convert a significant fraction of the incident energy flux from the solar wind[26]. Hence, future studies must directly explore the generation of current sheets and associated energy repartition with respect to the full and varied parameter space within the magnetosphere.

ACKNOWLEDGMENTS

I. Gingell is supported by the Royal Society University Research Fellowship URF\R1\191547. This study is also supported by NASA award #80NSSC19K0849.

DATA AVAILABILITY STATEMENT

The data that support the findings of this study are openly available at the MMS Science Data Center at the Laboratory for Atmospheric and Space Physics (LASP) hosted by the University of Colorado, Boulder (`https://lasp.colorado.edu/mms/sdc/public/`), reference numbers 27, 29–32, and NASA/GSFC's Space Physics Data Facility's OMNIWeb service (`https://omniweb.gsfc.nasa.gov/`, reference numbers 40–43.

AUTHOR DECLARATIONS

A. Conflicts of Interest

The authors have no conflicts to disclose.

REFERENCES

[1] F. Sahraoui, G. Belmont, J. Pinçon, L. Rezeau, A. Balogh, P. Robert, and N. Cornilleau-Wehrlin, "Magnetic turbulent spectra in the magnetosheath: new insights," Annales Geophysicae **22**, 2283–2288 (2004).

[2]O. Alexandrova, C. Lacombe, and A. Mangeney, "Spectra and anisotropy of magnetic fluctuations in the Earth's magnetosheath: Cluster observations," Annales Geophysicae **26**, 3585–3596 (2008), arXiv:0810.0675 [astro-ph].

[3]S. Y. Huang, F. Sahraoui, X. H. Deng, J. S. He, Z. G. Yuan, M. Zhou, Y. Pang, and H. S. Fu, "Kinetic Turbulence in the Terrestrial Magnetosheath: Cluster Observations," Astrophysical Journal Letters **789**, L28 (2014), arXiv:1312.5167 [astro-ph.SR].

[4]S. Y. Huang, L. Z. Hadid, F. Sahraoui, Z. G. Yuan, and X. H. Deng, "On the Existence of the Kolmogorov Inertial Range in the Terrestrial Magnetosheath Turbulence," Astrophysical Journal Letters **836**, L10 (2017), arXiv:1611.00199 [physics.space-ph].

[5]A. Chasapis, Y. Yang, W. H. Matthaeus, T. N. Parashar, C. C. Haggerty, J. L. Burch, T. E. Moore, C. J. Pollock, J. Dorelli, D. J. Gershman, R. B. Torbert, and C. T. Russell, "Energy Conversion and Collisionless Plasma Dissipation Channels in the Turbulent Magnetosheath Observed by the Magnetospheric Multiscale Mission," The Astrophysical Journal **862**, 32 (2018).

[6]W. H. Matthaeus, M. Wan, S. Servidio, A. Greco, K. T. Osman, S. Oughton, and P. Dmitruk, "Intermittency, nonlinear dynamics and dissipation in the solar wind and astrophysical plasmas," Philosophical Transactions of the Royal Society A: Mathematical, Physical and Engineering Sciences **373**, 20140154 (2015), https://royalsocietypublishing.org/doi/pdf/10.1098/rsta.2014.0154.

[7]W. H. Matthaeus and S. L. Lamkin, "Turbulent magnetic reconnection," The Physics of Fluids **29**, 2513–2534 (1986), https://aip.scitation.org/doi/pdf/10.1063/1.866004.

[8]V. Carbone, P. Veltri, and A. Mangeney, "Coherent structure formation and magnetic field line reconnection in magnetohydrodynamic turbulence," Physics of Fluids A **2**, 1487–1496 (1990).

[9]S. Servidio, W. H. Matthaeus, M. A. Shay, P. A. Cassak, and P. Dmitruk, "Magnetic Reconnection in Two-Dimensional Magnetohydrodynamic Turbulence," Physical Review Letters **102**, 115003 (2009).

[10]S. Donato, S. Servidio, P. Dmitruk, V. Carbone, M. A. Shay, P. A. Cassak, and W. H. Matthaeus, "Reconnection events in two-dimensional Hall magnetohydrodynamic turbulence," Physics of Plasmas **19**, 092307 (2012).

[11]L. Franci, S. S. Cerri, F. Califano, S. Landi, E. Papini, A. Verdini, L. Matteini, F. Jenko, and P. Hellinger, "Magnetic Reconnection as a Driver for a Sub-ion-scale Cascade in Plasma Turbulence," Astrophysical Journal Letters **850**, L16 (2017), arXiv:1707.06548 [physics.space-ph].

[12]T. D. Phan, G. Paschmann, C. Twitty, F. S. Mozer, J. T. Gosling, J. P. Eastwood, M. Øieroset, H. Rème, and E. A. Lucek, "Evidence for magnetic reconnection initiated in the magnetosheath," Geophysical Research Letters **34**, L14104 (2007).

[13]A. Retinò, D. Sundkvist, A. Vaivads, F. Mozer, M. André, and C. J. Owen, "In situ evidence of magnetic reconnection in turbulent plasma," Nature Physics **3**, 236–238 (2007).

[14]D. Sundkvist, A. Retinò, A. Vaivads, and S. D. Bale, "Dissipation in Turbulent Plasma due to Reconnection in Thin Current Sheets," Physical Review Letters **99**, 025004 (2007).

[15]E. Yordanova, Z. Vörös, A. Varsani, D. B. Graham, C. Norgren, Y. V. Khotyaintsev, A. Vaivads, E. Eriksson, R. Nakamura, P. A. Lindqvist, G. Marklund, R. E. Ergun, W. Magnes, W. Baumjohann, D. Fischer, F. Plaschke, Y. Narita, C. T. Russell, R. J. Strangeway, O. Le Contel, C. Pollock, R. B. Torbert, B. J. Giles, J. L. Burch, L. A. Avanov, J. C. Dorelli, D. J. Gershman, W. R. Paterson, B. Lavraud, and Y. Saito, "Electron scale structures and magnetic reconnection signatures in the turbulent magnetosheath," Geophysical Research Letters **43**, 5969–5978 (2016), arXiv:1706.04053 [physics.space-ph].

[16]Z. Vörös, E. Yordanova, A. Varsani, K. J. Genestreti, Y. V. Khotyaintsev, W. Li, D. B. Graham, C. Norgren, R. Nakamura, Y. Narita, F. Plaschke, W. Magnes, W. Baumjohann, D. Fischer, A. Vaivads, E. Eriksson, P.-A. Lindqvist, G. Marklund, R. E. Ergun, M. Leitner, M. P. Leubner, R. J. Strangeway, O. Le Contel, C. Pollock, B. J. Giles, R. B. Torbert, J. L. Burch, L. A. Avanov, J. C. Dorelli, D. J. Gershman, W. R. Paterson, B. Lavraud, and Y. Saito, "Mms observation of magnetic reconnection in the turbulent magnetosheath," Journal of Geophysical Research: Space Physics **122**, 11,442–11,467 (2017), https://agupubs.onlinelibrary.wiley.com/doi/pdf/10.1002/2017JA024535.

[17]T. D. Phan, J. P. Eastwood, M. A. Shay, J. F. Drake, B. U. Ö. Sonnerup, M. Fujimoto, P. A. Cassak, M. Øieroset, J. L. Burch, R. B. Torbert, A. C. Rager, J. C. Dorelli, D. J. Gershman, C. Pollock, P. S. Pyakurel, C. C. Haggerty, Y. Khotyaintsev, B. Lavraud, Y. Saito, M. Oka, R. E. Ergun, A. Retino, O. Le Contel, M. R. Argall, B. L. Giles, T. E. Moore, F. D. Wilder, R. J. Strangeway, C. T. Russell, P. A. Lindqvist, and W. Magnes, "Electron magnetic reconnection without ion coupling in Earth's turbulent magnetosheath," Nature **557**, 202–206 (2018).

[18]F. D. Wilder, R. E. Ergun, J. L. Burch, N. Ahmadi, S. Eriksson, T. D. Phan, K. A. Goodrich, J. Shuster, A. C. Rager, R. B. Torbert, B. L. Giles, R. J. Strangeway, F. Plaschke, W. Magnes, P. A. Lindqvist, and Y. V. Khotyaintsev, "The Role of the Parallel Electric Field in Electron-Scale Dissipation at Reconnecting Currents in the Magnetosheath," Journal of Geophysical Re-

search (Space Physics) **123**, 6533–6547 (2018).

[19] J. E. Stawarz, J. P. Eastwood, T. D. Phan, I. L. Gingell, M. A. Shay, J. L. Burch, R. E. Ergun, B. L. Giles, D. J. Gershman, O. Le Contel, P.-A. Lindqvist, C. T. Russell, R. J. Strangeway, R. B. Torbert, M. R. Argall, D. Fischer, W. Magnes, and L. Franci, "Properties of the Turbulence Associated with Electron-only Magnetic Reconnection in Earth's Magnetosheath," Astrophysical Journal Letters **877**, L37 (2019).

[20] I. Gingell, S. J. Schwartz, J. P. Eastwood, J. L. Burch, R. E. Ergun, S. Fuselier, D. J. Gershman, B. L. Giles, Y. V. Khotyaintsev, B. Lavraud, P.-A. Lindqvist, W. R. Paterson, T. D. Phan, C. T. Russell, J. E. Stawarz, R. J. Strangeway, R. B. Torbert, and F. Wilder, "Observations of Magnetic Reconnection in the Transition Region of Quasi-Parallel Shocks," Geophys. Res. Lett. **46**, 1177–1184 (2019), arXiv:1901.01076 [physics.space-ph].

[21] S. Wang, L.-J. Chen, N. Bessho, M. Hesse, L. B. Wilson, B. Giles, T. E. Moore, C. T. Russell, R. B. Torbert, and J. L. Burch, "Observational Evidence of Magnetic Reconnection in the Terrestrial Bow Shock Transition Region," Geophys. Res. Lett. **46**, 562–570 (2019), arXiv:1812.09337 [physics.space-ph].

[22] I. Gingell, S. J. Schwartz, J. P. Eastwood, J. E. Stawarz, J. L. Burch, R. E. Ergun, S. A. Fuselier, D. J. Gershman, B. L. Giles, Y. V. Khotyaintsev, B. Lavraud, P. A. Lindqvist, W. R. Paterson, T. D. Phan, C. T. Russell, R. J. Strangeway, R. B. Torbert, and F. Wilder, "Statistics of Reconnecting Current Sheets in the Transition Region of Earth's Bow Shock," Journal of Geophysical Research (Space Physics) **125**, e27119 (2020).

[23] Y. Matsumoto, T. Amano, T. N. Kato, and M. Hoshino, "Stochastic electron acceleration during spontaneous turbulent reconnection in a strong shock wave," Science **347**, 974–978 (2015), http://science.sciencemag.org/content/347/6225/974.full.pdf.

[24] I. Gingell, S. J. Schwartz, D. Burgess, A. Johlander, C. T. Russell, J. L. Burch, R. E. Ergun, S. Fuselier, D. J. Gershman, B. L. Giles, K. A. Goodrich, Y. V. Khotyaintsev, B. Lavraud, P.-A. Lindqvist, R. J. Strangeway, K. Trattner, R. B. Torbert, H. Wei, and F. Wilder, "MMS Observations and Hybrid Simulations of Surface Ripples at a Marginally Quasi-Parallel Shock," Journal of Geophysical Research (Space Physics) **122**, 11 (2017).

[25] N. Bessho, L.-J. Chen, S. Wang, M. Hesse, and L. B. Wilson III, "Magnetic reconnection in a quasi-parallel shock: Two-dimensional local particle-in-cell simulation," Geophysical Research Letters **46**, 9352–9361 (2019), https://agupubs.onlinelibrary.wiley.com/doi/pdf/10.1029/2019GL083397.

[26]S. J. Schwartz, H. Kucharek, C. J. Farrugia, K. Trattner, I. Gingell, R. E. Ergun, R. Strangeway, and D. Gershman, "Energy conversion within current sheets in the earth's quasi-parallel magnetosheath," Geophysical Research Letters **48**, e2020GL091859 (2021), e2020GL091859 2020GL091859, https://agupubs.onlinelibrary.wiley.com/doi/pdf/10.1029/2020GL091859.

[27]J. L. Burch, T. E. Moore, R. B. Torbert, and B. L. Giles, "Magnetospheric Multiscale Overview and Science Objectives," Space Science Reviews **199**, 5–21 (2016).

[28]C. T. Russell, B. J. Anderson, W. Baumjohann, K. R. Bromund, D. Dearborn, D. Fischer, G. Le, H. K. Leinweber, D. Leneman, W. Magnes, J. D. Means, M. B. Moldwin, R. Nakamura, D. Pierce, F. Plaschke, K. M. Rowe, J. A. Slavin, R. J. Strangeway, R. Torbert, C. Hagen, I. Jernej, A. Valavanoglou, and I. Richter, "The Magnetospheric Multiscale Magnetometers," Space Science Reviews **199**, 189–256 (2016).

[29]R. E. Ergun, S. Tucker, J. Westfall, K. A. Goodrich, D. M. Malaspina, D. Summers, J. Wallace, M. Karlsson, J. Mack, N. Brennan, B. Pyke, P. Withnell, R. Torbert, J. Macri, D. Rau, I. Dors, J. Needell, P. A. Lindqvist, G. Olsson, and C. M. Cully, "The Axial Double Probe and Fields Signal Processing for the MMS Mission," Space Science Reviews **199**, 167–188 (2016).

[30]P.-A. Lindqvist, G. Olsson, R. B. Torbert, B. King, M. Granoff, D. Rau, G. Needell, S. Turco, I. Dors, P. Beckman, J. Macri, C. Frost, J. Salwen, A. Eriksson, L. Åhlén, Y. V. Khotyaintsev, J. Porter, K. Lappalainen, R. E. Ergun, W. Wermeer, and S. Tucker, "The spin-plane double probe electric field instrument for mms," Space Science Reviews **199**, 137–165 (2016).

[31]R. B. Torbert, C. T. Russell, W. Magnes, R. E. Ergun, P.-A. Lindqvist, O. LeContel, H. Vaith, J. Macri, S. Myers, D. Rau, J. Needell, B. King, M. Granoff, M. Chutter, I. Dors, G. Olsson, Y. V. Khotyaintsev, A. Eriksson, C. A. Kletzing, S. Bounds, B. Anderson, W. Baumjohann, M. Steller, K. Bromund, G. Le, R. Nakamura, R. J. Strangeway, H. K. Leinweber, S. Tucker, J. Westfall, D. Fischer, F. Plaschke, J. Porter, and K. Lappalainen, "The FIELDS Instrument Suite on MMS: Scientific Objectives, Measurements, and Data Products," Space Science Reviews **199**, 105–135 (2016).

[32]C. Pollock, T. Moore, A. Jacques, J. Burch, U. Gliese, Y. Saito, T. Omoto, L. Avanov, A. Barrie, V. Coffey, J. Dorelli, D. Gershman, B. Giles, T. Rosnack, C. Salo, S. Yokota, M. Adrian, C. Aoustin, C. Auletti, S. Aung, V. Bigio, N. Cao, M. Chandler, D. Chornay, K. Christian, G. Clark, G. Collinson, T. Corris, A. De Los Santos, R. Devlin, T. Diaz, T. Dickerson, C. Dickson, A. Diekmann, F. Diggs, C. Duncan, A. Figueroa-Vinas, C. Firman, M. Freeman, N. Galassi, K. Garcia, G. Goodhart, D. Guererro, J. Hageman, J. Hanley, E. Hemminger, M. Holland,

M. Hutchins, T. James, W. Jones, S. Kreisler, J. Kujawski, V. Lavu, J. Lobell, E. LeCompte, A. Lukemire, E. MacDonald, A. Mariano, T. Mukai, K. Narayanan, Q. Nguyan, M. Onizuka, W. Paterson, S. Persyn, B. Piepgrass, F. Cheney, A. Rager, T. Raghuram, A. Ramil, L. Reichenthal, H. Rodriguez, J. Rouzaud, A. Rucker, Y. Saito, M. Samara, J.-A. Sauvaud, D. Schuster, M. Shappirio, K. Shelton, D. Sher, D. Smith, K. Smith, S. Smith, D. Steinfeld, R. Szymkiewicz, K. Tanimoto, J. Taylor, C. Tucker, K. Tull, A. Uhl, J. Vloet, P. Walpole, S. Weidner, D. White, G. Winkert, P.-S. Yeh, and M. Zeuch, "Fast Plasma Investigation for Magnetospheric Multiscale," Space Science Reviews **199**, 331–406 (2016).

[33] M. Peredo, J. A. Slavin, E. Mazur, and S. A. Curtis, "Three-dimensional position and shape of the bow shock and their variation with Alfvenic, sonic and magnetosonic Mach numbers and interplanetary magnetic field orientation," Journal of Geophysical Research **100**, 7907–7916 (1995).

[34] E. C. Roelof and D. G. Sibeck, "Magnetopause shape as a bivariate function of interplanetary magnetic field B_z and solar wind dynamic pressure," Journal of Geophysical Research **98**, 21421–21450 (1993).

[35] P. Robert, M. W. Dunlop, A. Roux, and G. Chanteur, "Accuracy of Current Density Determination," ISSI Scientific Reports Series **1**, 395–418 (1998).

[36] B. U. Ö. Sonnerup and M. Scheible, "Minimum and Maximum Variance Analysis," ISSI Scientific Reports Series **1**, 185–220 (1998).

[37] T. D. Phan, M. A. Shay, J. T. Gosling, M. Fujimoto, J. F. Drake, G. Paschmann, M. Oieroset, J. P. Eastwood, and V. Angelopoulos, "Electron bulk heating in magnetic reconnection at Earth's magnetopause: Dependence on the inflow Alfvén speed and magnetic shear," Geophysical Research Letters **40**, 4475–4480 (2013).

[38] E. Yordanova, Z. Vörös, S. Raptis, and T. Karlsson, "Current sheet statistics in the magnetosheath," Frontiers in Astronomy and Space Sciences **7**, 2 (2020).

[39] I. Gingell, L. Sorriso-Valvo, D. Burgess, G. de Vita, and L. Matteini, "Three-dimensional simulations of sheared current sheets: transition to turbulence?" Journal of Plasma Physics **83**, 705830104 (2017).

[40] R. P. Lepping, M. H. Acũna, L. F. Burlaga, W. M. Farrell, J. A. Slavin, K. H. Schatten, F. Mariani, N. F. Ness, F. M. Neubauer, Y. C. Whang, J. B. Byrnes, R. S. Kennon, P. V. Panetta, J. Scheifele, and E. M. Worley, "The Wind Magnetic Field Investigation," Space Science Reviews **71**, 207–229 (1995).

[41]K. W. Ogilvie, D. J. Chornay, R. J. Fritzenreiter, F. Hunsaker, J. Keller, J. Lobell, G. Miller, J. D. Scudder, J. Sittler, E. C., R. B. Torbert, D. Bodet, G. Needell, A. J. Lazarus, J. T. Steinberg, J. H. Tappan, A. Mavretic, and E. Gergin, "SWE, A Comprehensive Plasma Instrument for the Wind Spacecraft," Space Science Reviews **71**, 55–77 (1995).

[42]C. W. Smith, J. L'Heureux, N. F. Ness, M. H. Acuña, L. F. Burlaga, and J. Scheifele, "The ACE Magnetic Fields Experiment," Space Science Reviews **86**, 613–632 (1998).

[43]D. J. McComas, S. J. Bame, P. Barker, W. C. Feldman, J. L. Phillips, P. Riley, and J. W. Griffee, "Solar Wind Electron Proton Alpha Monitor (SWEPAM) for the Advanced Composition Explorer," Space Science Reviews **86**, 563–612 (1998).